Combustion and Flame 161 (2014) 1038–1047

Contents lists available at ScienceDirect

Combustion and Flame

journal homepage: www.elsevier.com/locate/combustflame

Thermochemistry of the combustion of gas phase and condensed phase detonation products in an explosive fireball

Luke S. Lebel [a,*], Patrick Brousseau [b], Lorne Erhardt [c], William S. Andrews [a]

[a] Chemistry and Chemical Engineering, Royal Military College of Canada, PO Box 17000, Kingston, ON K7K 7B4, Canada
[b] Energetic Materials Section, Defence Research Development Canada – Valcartier, 2459 Pie-XI Blvd North, Québec, QC G3J 1X5, Canada
[c] Radiological Analysis and Defence Group, Defence Research Development Canada – Ottawa, 3701 Carling Ave, Ottawa, ON K1A 0Z4, Canada

ARTICLE INFO

Article history:
Received 26 July 2013
Received in revised form 24 September 2013
Accepted 23 October 2013
Available online 13 November 2013

Keywords:
Fireball mechanics
Thermochemistry
Turbulence
Heterogeneous combustion

ABSTRACT

This paper uses the thermochemical behaviour of reacting species to differentiate between the combustion of gas phase and condensed phase detonation products in the fireball of an explosion. Experiments were carried out involving the detonation 15 g charges of C-4 and Detasheet-C explosives in a closed vessel. The initial partial pressure of oxygen in the vessel was varied in order to control the extent of the secondary afterburn reactions, and the total heat release was measured using the calorimeter that contained the closed vessel. A simple model that independently describes the evolution of heat from the gas phase and condensed phase detonation products as a function of oxygen consumption was developed, and was used to show that condensed phase products react much more effectively in the fireball than gas phase reactions, because the transport properties of particulates entrained in a turbulent flow gives them an advantage when it comes to the manner in which they mix with the surrounding air. An additional set of trials employing the entrainment of an external combustible material further confirms the importance of particle combustion in explosive fireballs.

1. Introduction

When high explosives are detonated, they often produce energetic, secondary fireballs. In many cases, the proportion of the total combustion energy released, assuming the detonation products could react completely with air, could exceed what would be liberated during the initial detonation. For example, with C-4, the heat of detonation is only 44% the total heat of combustion, and for Detasheet-C, it is only 32% [1].

$$\Delta H_{c,x} = \Delta H_{d,x} + \Delta H_{ab,x} \quad (1)$$

The mechanical energy carried away by the blast has been the traditional focus of explosives research, because it is this portion that does the useful work in civil, mining, or military applications. However, with the advent of thermobaric charges and enhanced blast weapons, where the afterburn reactions that occur behind the initial shock wave can sustain the duration of the positive impulse phase of a blast, the phenomena associated with the fireball have become increasingly important [2].

Considerable advances have been made in recent years in describing the dynamic energy release that occurs in the fireball. In the work by Balakrishnan [3,4], in particular, modern computational techniques have been applied in order to describe the fireball mechanics in 3 dimensions, building on previous work by Brode [5], Ansimov and Zeldovich [6], and Kuhl et al. [7]. Frost et al. [8] also attempted to model the expansion, instabilities, and turbulent mixing of the fireball while investigating heterogeneous explosives, where reactive particulates were suspended in an explosive matrix and detonated.

However, in terms of homogeneous explosives, the interrelationship between transport and chemical reaction, and how they may differ between different types of reacting species, has largely been neglected. The complex mixing models developed by Balakrishnan, for example, have largely assumed that the afterburn is entirely transport-controlled, with infinitely fast reaction kinetics and no differentiation between different chemical species [3,4]. McNesby et al. [9], on the other hand, considered the kinetics of the afterburn reactions, but modelled them as a spatially homogeneous system without taking into account mixing and transport, and with no mention of the behaviour of the condensed phase carbonaceous soot.

In either case, the important distinction between the combustion of gas phase species (e.g., CO, H_2, CH_4, NH_3, etc.), and condensed phase species (e.g., carbonaceous soot), has not been taken into account, and the present work aims to show that

* Corresponding author. Present address: Fuel and Fuel Channel Safety Branch, Atomic Energy of Canada Limited, AECL-CRL, Stn 88, Chalk River, ON K0J 1J0, Canada.
E-mail addresses: luke.lebel@rmc.ca, lebell@aecl.ca (L.S. Lebel), patrick.brousseau@drdc-rddc.gc.ca (P. Brousseau), lorne.erhardt@drdc-rddc.gc.ca (L. Erhardt), andrews-w@rmc.ca (W.S. Andrews).

0010-2180/$ - see front matter Crown Copyright © 2013 Published by Elsevier Inc. on behalf of The Combustion Institute. All rights reserved.
http://dx.doi.org/10.1016/j.combustflame.2013.10.024

Nomenclature

$\boldsymbol{A}$	matrix relating reaction extent vector to vector of oxygen-weighted and energy-weighted total reaction extents
a	ratio of oxygen stoichiometry coefficients
b	ratio of heats of reaction
C_c	Cunningham slip correction factor
D	diffusivity (m^2 s)
d_p	particle diameter
E_r	total rotational kinetic energy of a turbulent eddy (J)
f	fractional rate at which oxygen is consumed in gas phase reactions
f_m	mass fraction of combustible detonation products
ΔH_{ab}	heat of afterburn (kJ mol^{-1})
ΔH_c	heat of combustion (kJ mol^{-1})
ΔH_d	heat of detonation (kJ mol^{-1})
ΔH_r	heat of reaction (kJ mol^{-1})
j	mass flux (kg m^{-2} s^{-1})
$k(\ell)$	specific turbulent kinetic energy at length scale ℓ (m^2 s^{-2})
ℓ	length scale (m)
n	moles of reacting species (mol)
Δn	moles consumed by reaction (mol)
Q	heat release (kJ)
R	radius of curvature for a circulating flow (m)
r	rate of reaction (mol s^{-1})
v	effective interfacial mixing velocity (m s^{-1})
v_t	tangential velocity of a circulating flow (m s^{-1})

Greek

η	energy-weighted total reaction extent
ν	stoichiometric coefficient
ξ	individual reaction extent
$\boldsymbol{\xi}$	vector containing individual reaction extents
μ	dynamic viscosity (Pa s)
ρ	density (kg m^{-3})
τ	relaxation time of a particle
χ	oxygen-weighted total reaction extent
ω	angular velocity of a turbulent eddy (rad s^{-1})

Subscript

c	condensed phase
crit	critical transition point
d	molecular diffusion
dt	duct tape
g	gas phase
i	initial
k	Kolmogorov
meas	measured
O_2	oxygen
p	particle
x	explosives

Superscript

$*$	at stoichiometry

nuances in the way that particulates mix in the turbulent flow gives them an advantage that allows them to react with oxygen at considerably higher rates than gas phase species.

2. Gas-particle mixing in a turbulent environment

In a turbulent flow, as would be encountered in a fireball, the gases mix together because of turbulent shear. High shear at the interface between detonation product gases and air makes the flow unstable, and causes mixing analogous to a Kelvin-Hemholtz instability [10]. This results in circulation between the two interfaces. For the gas phase reactions to occur, intimate molecular contact between species is required, and on the micro-scale the only way to achieve this is through molecular diffusion. Bulk phase mixing occurs, and the gas phase reactions would, of course, occur along the interface between gases, but the ingress of species into the opposite phase, and therefore the thickness of the reaction zone, would be limited by molecular diffusion.

Particulates, on the other hand, have a mass, and have inertia relative to the gas in which they are suspended, and in an accelerating flow (i.e., when the gas flow makes a turn), they will deviate from the streamlines of the flow based on their relaxation time, $\tau = \rho_p d_p^2 C_c / 18\ \mu$ [11,12]. This means that particulates can get thrown out of the carrier gas, and cross fluid–fluid boundaries as illustrated in Fig. 1. In turbulent flow fields, particles are known to be strongly influenced by small scale turbulence, and can exhibit erratic flow paths and be subject to intense accelerations as a result [13]. As the gases mix together, particles will escape from the detonation products and cross into the air. This allows them to come into contact more efficiently with oxygen compared to molecular diffusion, which allows for a much thicker reaction zone, and thus enhances the rate at which they are consumed.

To express this in more formal terms, the radial velocity of a particle in a circulating fluid is based on the tangential velocity of the gas, as well as the radius of curvature of the circulation [11,12]. This defines the speed at which particles deviate from the streamlines of the gases, and as such the speed at which they can ingress into more oxygen-rich regions.

$$v_p = \tau \frac{v_t^2}{R} \tag{2}$$

The relaxation time, τ, contains all of the information about the particle transport properties, including particle size and density, drag, and fluid viscosity. The circulation of the fluid is a manifestation of the turbulence of the flow, and so one would expect the particulates' radial velocities to be a function of both the turbulent kinetic energy and turbulent length scale. To get an idea of the general behaviour of particulates in turbulence, consider an aerosol-laden cylindrical eddy rotating like a rigid body with an angular velocity ω. The outward radial velocity of the particulates could then be expressed by:

$$v_p = \tau R \omega^2 \tag{3}$$

The rotational kinetic energy of the cylindrical eddy, with radius R and length h would therefore be:

$$E_r = \frac{\pi}{4} \rho_g h R^4 \omega^2 \tag{4}$$

The turbulent kinetic energy of a fluid is contained in the rotational energy of individual eddies rotating over a spectrum of different length scales, and so normalizing Eq. (4) by the mass of the cylindrical eddy would essentially give its contribution to the turbulent kinetic energy for an eddy of a particular size.

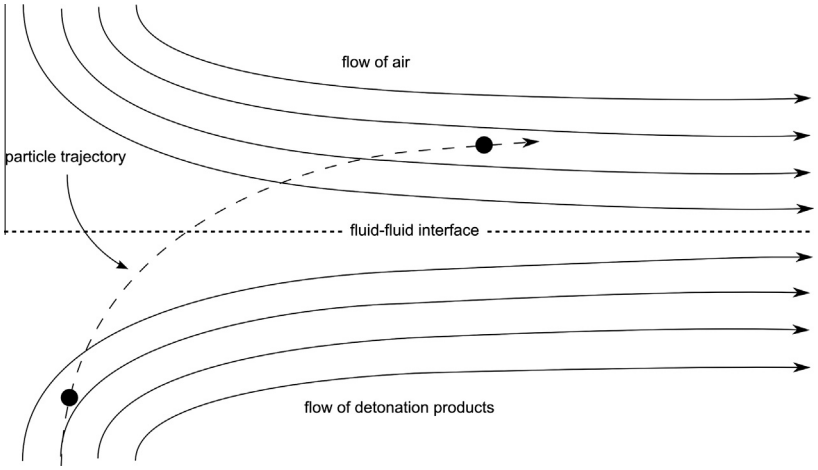

Fig. 1. Particles have inertia, and do not exactly follow the streamlines of the carrier gas.

$$k(R) = \frac{E_r}{\pi \rho_g h R^2} = \frac{1}{4} R^2 \omega^2 \tag{5}$$

By combining Eqs. (3) and (5), and defining the length scale for the particulate mixing velocity as the eddy diameter, $\ell_p = 2R$, the following expression that describes the radial particle velocity at the edge of an eddy as a function of turbulent kinetic energy can be obtained:

$$v_p = 8\tau \frac{k(\ell_p)}{\ell_p} \tag{6}$$

This is essentially the effective velocity for particle mixing in a turbulent field, and Eq. (6) implies that for more intense turbulence, and for turbulence at smaller length scales, the speed at which particles can deviate from the streamlines of their carrier gases and ingress into more oxygen rich areas increases. In contrast, smaller and lighter particulates, especially those in the submicron size range, will much more closely follow the motion of the surrounding gas compared to larger, heavier particles, and therefore have much smaller values for v_p. These will likely be more affected by diffusive processes and Brownian motion, as opposed to the inertial effects that have been described thus far.

For gaseous species, bulk turbulent mixing will certainly occur between the fuel-rich, detonation product steam and the surrounding air, but the actual combustion will be limited to microscale regions at the interfaces between the two fluids, and ultimately, will be driven by molecular diffusion. The diffusive mass flux, j, for gaseous fuel across this interface would be:

$$j = -\rho_g D \frac{df_m}{dx} \tag{7}$$

where f_m is the mass fraction of combustible gaseous detonation products that are diffusing across the fuel–air interface the oxygen-rich region with a diffusivity D [14].

The effective diffusive velocity of these molecular species can be taken as the ratio of the mass flux in Eq. (7) over the gas density. In a turbulent field, the smallest eddies are typically on the order of the Kolmogorov length scale, $\ell_k = (\nu^3/\varepsilon)^{1/4}$, after which viscous and diffusive forces dominate [15]. A rough estimate of the effective diffusive velocity can therefore be obtained by assuming that the concentration gradient varies from $f_m = 1$ to $f_m = 0$ over a diffusion length, ℓ_d, that is of the same order as the Kolmogorov length scale.

$$v_d = \frac{j}{\rho_g} \sim \frac{D}{\ell_d} \tag{8}$$

Eqs. (6) and (8) each give a different measure of the microscale driving forces, respectively, for particulate mixing and gas mixing in a turbulent environment, and factors that influence which mode of mixing dominates can be determined by taking their ratio.

$$\frac{v_p}{v_d} \sim \frac{8\tau k(\ell_p)}{D} \left(\frac{\ell_d}{\ell_p}\right) \tag{9}$$

From this expression, it is clear that as the turbulent kinetic energy increases, the relative effectiveness of particulate mixing would increase as well. Both v_p and v_d are inversely proportional to their respective length scales, but since the most effective mixing in either case occurs when these length scales are small, one could consider them both to be approximately the same and on the same order as the size of the smallest eddies in the turbulent field. At temperatures at about 1600 K, which have been observed in an explosive fireball's interior [16], the binary diffusion coefficient for the detonation product gases in air would be on the order of 1×10^{-4} m^2 s^{-1} [17], while the relaxation times, also at 1600 K, for 1 μm and 10 μm (aerodynamic diameter) particles would be on the order of 5×10^{-7} s and 5×10^{-5} s, respectively [11]. For v_p to be greater than v_d, the turbulent kinetic energies of the smallest eddies would have to be on the order of 25 m^2 s^{-2} for 1 μm particles and 0.25 m^2 s^{-2} for 10 μm particles. This corresponds to turbulence whose velocity magnitudes are on the order of 5 m s^{-1} and 0.5 m s^{-1}. For explosive fireballs that expand into the surrounding air at many times the speed of sound, achieving turbulence at this level or higher is quite conceivable.

3. Experimental

Calorimetry experiments were carried out at the Royal Military College of Canada, and involved detonating 15 g explosive charges in a sealed 5.54 L detonation vessel. Prior to each trial, the detonation vessel was loaded with nitrogen and oxygen gas, at a predetermined ratio, to an initial total pressure of about 650 kPa (absolute). The calorimeter, of which the closed detonation vessel was the central component, was used to measure the total quantity of energy released in each trial. Experimental conditions were chosen, and oxygen was added in sufficient quantities, so that a specific degree of afterburn, generally ranging between 0% to slightly over 100% stoichiometric combustion of the secondary afterburn reactions, could be achieved. Although carrying out these

detonations in a closed vessel will not exactly simulate a real, open air explosion, e.g., blast wave reflections, limits to free expansion, vessel walls potentially acting as a heat sink, etc., the charge is small enough relative to the free environment that results should be reasonably close.

3.1. Explosives

Two types of explosive (C-4 and Detasheet-C) were employed in this experimental program, and charges were initiated using Teledyne RISI RP-83 exploding bridgewire detonators. The explosive and detonator were held together with standard duct tape, and not otherwise confined. The charges were suspended from the detonator lead wires in the center of the detonation vessel, and were initiated inside the closed vessel using a Teledyne RISI FS-61B firing unit.

3.2. Calorimetry

A specialized calorimeter [18] was employed for the thermochemical measurements, and is shown schematically in Fig. 2.

There were three main parts to the calorimeter. The actual explosions were carried out in the thick-walled, stainless steel detonation vessel, which was, in turn, immersed in 12.0 L of water in an inner jacket. Heat released from the explosions was absorbed by the water, and the temperature rise was measured by an Omega Engineering P-M-1/10-1/8-60-P-3 RTD temperature probe connected to a National Instruments Compact RIO. The inner jacket was insulated to reduce energy loss, and was contained in the outer jacket, which was filled with water held at a constant 25.500 °C. The outer jacket provided an isothermal environment for the calorimetry trials. The observed temperature rises were compared to those observed from a series of benzoic acid calibration trials, from which a measured heat release, Q_{meas}, could be obtained.

3.3. Entrainment of external materials

As part of a concurrent study to investigate the effects of soil entrainment in explosive fireballs [19,20], during most trials, different types of soil were added to the bottom of the vessel. Two of the soil types, quartz sand and clay, were non-interacting, and would not have affected the total energy release. This was not true of black earth, however, a third type of soil that was obtained from Black Earth Humates Ltd., because it was composed of combustible organic matter. When entrained in the turbulent fireball following the blasts, it would have been able to participate in the secondary combustion reactions.

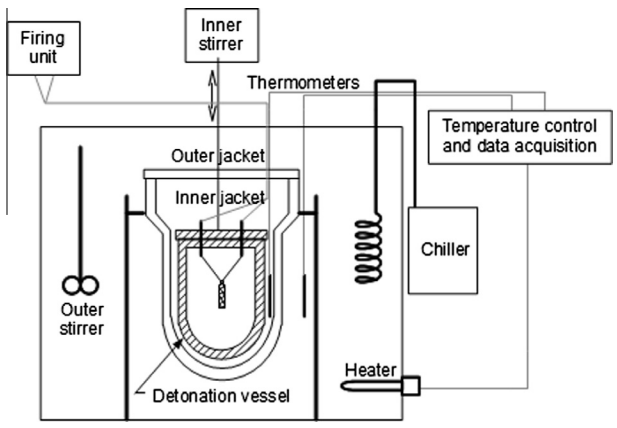

Fig. 2. Schematic of the calorimeter.

As will be presented in this paper, major differences have been observed with regards to the thermochemical behaviour of gas-particle combustion versus gas–gas combustion, and the addition of external combustible material, beyond what is generated from the explosives, allows for better confirmation of the conclusions.

4. Calorimetry results

Calorimeter measurements are available for 50 shots in total, and the total heat release from C-4 and detasheet as a function of the initial partial pressure of oxygen in the detonation vessel are shown in Fig. 3.

A clear trend is observed in the data, where the amount of liberated heat increased directly with the amount of available oxygen. When trials were carried out under nitrogen, independent of whatever soil was present, data points were fairly tightly grouped. The heat of detonation was measured as 5.1 ± 0.2 kJ g^{-1} for C-4 and as 4.5 ± 0.2 kJ g^{-1} for detasheet.

The addition of oxygen to the vessel allowed the secondary combustion of the detonation products to proceed, thereby allowing more energy to be liberated. However, this did not proceed at a universal rate. For example, since the detasheet had a lower oxygen balance than the C-4, a higher proportion of its total combustion energy was released during the afterburn phase and less during the initial detonation phase. In fact, detasheet was capable of releasing more energy than C-4 when presented with enough oxygen, as evidenced by the maximum measured heat releases.

Although most of the soil types would not have participated in the secondary combustion reactions, black earth did. The total heat released from several of the trials can be seen below the general trend, and they correspond to the trials with black earth. For the trials carried out with an initial partial pressure of oxygen of 140 kPa, afterburn reactions released about 37% less energy for C-4, and 26% less energy for detasheet, as compared with baseline trials and trials carried out with other types of soil.

5. Thermochemical predictions using cheetah code

The starting materials, or fuel, for the secondary combustion reactions are the underoxidized detonation products. To predict the composition of these, as well as other detonation properties, the thermochemical solver, CHEETAH, developed at Lawrence Livermoore National Laboratory [21], was used. The code is an advanced thermodynamic equilibrium solver that is capable of predicting the composition of products after the initial detonation, but prior to any further reaction with atmospheric oxygen. Simulations

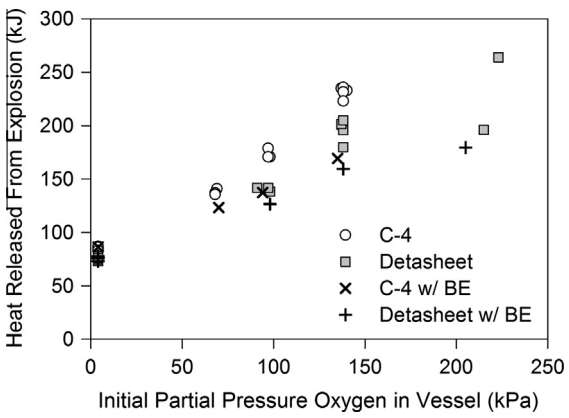

Fig. 3. Energy release from explosives as a function of the initial oxygen partial pressure.

were run using a copy of CHEETAH at DRDC Valcartier, and the thermochemical properties that were obtained are given in Tables 1–5. Among other things, the code predicted heats of detonation of 5.4 kJ-g^{-1} and 4.5 kJ-g^{-1} for C-4 and detasheet, respectively, which compare quite well with the values of 5.1 ± 0.2 kJ-g^{-1} and 4.5 ± 0.2 kJ-g^{-1} measured for these explosives.

Tables 1 and 2 give the composition of the explosives, in terms of their explosive ingredients as well as any fillers or additives. These values essentially represent the input to the CHEETAH code. Table 3 gives the different parameters, like the pressure and density, calculated at the Chapman-Jouguet condition, as well as the calculated shock velocity and the temperature at which the detonation product equilibrium is assumed to freeze-out. Table 4 gives an abbreviated list of detonation products and their relative compositions at both the C-J state and final freeze-out condition. The most important components out of the 63 considered by CHEETAH are given. Finally, Table 5 gives the heat of combustion, heat of detonation, and heat of afterburn for the explosives. The heat of afterburn, specifically, is also divided into the portion resulting from the condensed phase detonation products, e.g., carbonaceous soot, and the portion from the gas phase detonation products.

Table 1
Thermochemical properties of the components of C-4 [1,17,21].

Component	Chemical formula	Mass fraction	Heat of formation (kJ mol^{-1})
RDX	$C_3H_6N_6O_6$	0.910	+69
Polyisobutylene	$(C_4H_8)_n$	0.021	−88
Fuel oil	$\sim C_{10}H_{16}$	0.016	+29
DEH sebacate	$C_{26}H_{50}O_4$	0.053	−1335
Total	$C_{3.86}H_{7.57}N_{5.22}O_{5.32}$	1.000	+19

Oxygen balance: −46.6%

Table 2
Thermochemical properties of the components of Detasheet-C [1,17,21].

Component	Chemical formula	Mass fraction	Heat of formation (kJ mol^{-1})
PETN	$C_5H_8N_8O_{12}$	0.630	−527
NC (12.6% N)	$(C_6H_{7.55}N_{2.45}O_{12})_n$	0.080	−708
ATBC	$C_{20}H_{34}O_8$	0.290	−1820
Total	$C_{8.69}H_{14.19}N_{2.89}O_{10.84}$	1.000	−855

Oxygen balance: −65.6%.

Table 3
Detonation parameters, as calculated by CHEETAH.

Parameter	C-4	Detasheet
Shock velocity	8.03 km s^{-1}	7.09 km s^{-1}
C-J pressure	24.69 GPa	17.93 GPa
C-J temperature	3762 K	3099 K
Freeze-out temperature	2145 K	2145 K

Table 4
Product compositions at C-J state and freeze-out temperature, as calculated by CHEETAH.

Species	C-J State		Freeze-out	
	C-4	Detasheet	C-4	Detasheet
CO_2	1.63	3.39	1.38	3.09
H_2O	1.33	3.00	1.92	4.06
N_2	2.42	1.26	2.55	1.37
CO	0.03	0.05	0.62	0.58
H_2	0.09	0.15	0.59	0.69
CH_4	0.31	0.72	0.52	0.96
NH_3	0.37	0.36	0.12	0.15
Other	0.64	1.00	0.03	0.09
$C_{(s)}$	1.01	3.09	1.29	3.96

Table 5
Heats of reaction and oxygen stoichiometry at different stages of the explosion, using freeze-out equilibrium composition.

Reaction	Oxygen stoichiometry		Heat of reaction (kJ mol^{-1})	
	C-4	Detasheet	C-4	Detasheet
Total combustion	3.09	6.82	−2620	−4595
Detonation	–	–	−1144	−1493
Afterburn[a]	3.09	6.82	−1476	−3102
– For gaseous products[a]	*1.80*	*2.86*	*−967*	*−1543*
– For solid products[a]	*1.29*	*3.96*	*−509*	*−1559*

Heat of afterburn = afterburn for gaseous products + afterburn for solid products.
[a] These are all given in terms of complete combustion to CO_2, H_2O, etc., as opposed to partial combustion to CO or other partly oxidized species.

6. Thermochemical model of secondary combustion

A large number of detonation products can be produced during the initial detonation phase of an explosion, and many of those would react with oxygen in the air as they expand outward. The thermodynamic end state of the reacting species is dictated by the equilibrium conditions involved. This paper, however, will argue that the transport of species is the rate limiting step, and that certain species can react with oxygen more efficiently and achieve that thermodynamic end state before others. The basic hypothesis is that, in the highly turbulent flow fields that follow a detonation, condensed phase material in the form of particulates will mix with the surrounding air in a physically different way than gas phase species. The argument that will be made is that particulates, as a result of some of the unique aspects of aerosol transport, will actually be able to enter deeper into oxygen-rich areas, continually exposing fresh carbonaceous soot to oxygen, therefore allowing them to react at a higher rate.

The goal in this section is to develop a thermochemical model that can describe the overall secondary combustion process in as simple a formulation as possible. From the data that has been collected, a full analysis of all reaction pathways would not be possible, but it will be shown that employing lumped parameter model that treats all reactions as either a condensed phase or gas phase reaction still captures the essential phenomena. Ultimately, carbonaceous soot would react with oxygen to produce carbon dioxide. However, carbon monoxide would be an intermediate in that reaction, and on the microscale interfaces between soot particulates and air, one would expect the carbon monoxide to be initially evolved after the oxygen reacts with the carbon.

$$C_{(s)} + \frac{1}{2}O_2 \rightarrow CO \tag{10}$$

The carbon monoxide produced here from secondary combustion, along with the CO, H_2, CH_4, NH_3, and all the other underoxidized products produced from the initial detonation, can all undergo combustion in the fireball as well.

$$CO + \frac{1}{2}O_2 \rightarrow CO_2 \tag{11a}$$

$$H_2 + \frac{1}{2}O_2 \rightarrow H_2O \tag{11b}$$

$$CH_4 + 2O_2 \rightarrow CO_2 + 2H_2O \tag{11c}$$

$$NH_3 + \frac{3}{4}O_2 \rightarrow \frac{1}{2}N_2 + \frac{3}{2}H_2O \tag{11d}$$

This analysis uses the same assumption as Balakrishnan [3,4] in ignoring kinetic limits for the gas phase species, as reactions in a flame are typically diffusion controlled, but goes farther to assert that the mixing processes involved in gas-particle reactions involve fundamentally different mechanisms (e.g., Brownian motion, centrifugal effect in turbulence) than those involved in gas–gas reactions (e.g., molecular diffusion, turbulent bulk mixing). For the balance of this paper, therefore, it will be assumed that reactions involving different gas phase species will be all the same, but that these will be different from reactions involving condensed phase particulates. As such, all of the different gas phase detonation products can be taken together, and considered as an 'average' CHNO gas.

$$C_xH_yN_wO_z + v_{O2,g}O_2 \rightarrow xCO_2 + \frac{y}{2}H_2O + \frac{w}{2}N_2 \tag{12}$$

where $v_{O2,g}$ is the stoichiometric coefficient for oxygen for the gas phase reactions.

Likewise, with the soot, along with the tape used to wrap the charge, an average empirical chemical formula can be used as well.

$$C_xH_yN_wO_z + v_{O2,c}O_2 \rightarrow xCO + \frac{y}{2}H_2O + \frac{w}{2}N_2 \tag{13}$$

where $v_{O2,c}$ is the stoichiometric coefficient for oxygen for the condensed phase reactions.

Consider the case where gas phase species are reacting in the fireball at a rate, r_g, and condensed phase species are reacting at r_c. Or more precisely, for r_g and r_c, consider the rates at which oxygen is consumed by the respective reactions. The fractional rate, f, at which oxygen is consumed in the gas reactions relative to the total rate at which oxygen is being consumed, can therefore be defined as:

$$f = \frac{r_g}{r_c + r_g} \tag{14}$$

If a volume contains both detonation products and air, then the rate that the detonation products are consumed will be directly related to the rate of oxygen consumption by:

$$dn_g = f\frac{1}{v_{O2,g}}dn_{O2} \tag{15a}$$

$$dn_c = (1-f)\frac{1}{v_{O2,c}}dn_{O2} \tag{15b}$$

where n_g is moles of the gas phase reactants, n_c is moles of condensed phase reactants, and n_{O2} is moles of oxygen.

At any instant, a certain proportion of the gas phase or condensed phase material will have reacted. This can be tracked with the reaction extents, ξ_g and ξ_c, where an extent of $\xi = 0$ implies that none of the material has reacted yet, while an extent of $\xi = 1$ implies that it has all been consumed.

$$\xi_g = 1 - \frac{n_g}{n_{x,i}} \tag{16a}$$

$$\xi_c = 1 - \frac{n_c}{n_{x,i}} \tag{16b}$$

where $n_{x,i}$ is the initial moles of explosives. Note that as written, the generic CHNO gas phase and condensed phase compounds are defined to be in a 1:1 molar ratio with the original explosives. As a result, $n_{g,i} = n_{c,i} = n_{x,i}$.

The reaction extents themselves are continually changing as material is consumed in the fireball. Their rate of change can also be related to the rate of oxygen consumption by:

$$d\xi_g = -\frac{1}{n_{x,i}}dn_g = f\frac{1}{v_{O2,g}n_{x,i}}dn_{O2} \tag{17a}$$

$$d\xi_c = -\frac{1}{n_{x,i}}dn_c = (1-f)\frac{1}{v_{O2,c}n_{x,i}}dn_{O2} \tag{17b}$$

These last expressions define the differential reaction extent in terms of the differential rate of oxygen consumption. The total quantity of oxygen that has been consumed in the fireball can also be defined as the sum of the amount of oxygen consumed by each of the different classes of reacting species.

$$-\Delta n_{O2} = n_{x,i}(v_{O2,g}\xi_g + v_{O2,c}\xi_c) \tag{18}$$

When the secondary combustion reactions have gone to completion ($\xi_g = \xi_c = 1$), a maximum quantity of oxygen, Δn^*_{O2}, has been consumed. The amount of oxygen that has been consumed at any instant is always less than this, but normalizing the one by the other yields the oxygen-weighted total reaction extent, χ. This is a measure of the total reaction extent, based on oxygen consumption, for the gas phase and condensed phase combustion reactions together.

$$\chi = \frac{\Delta n_{O2}}{\Delta n^*_{O2}} = a\xi_g + (1-a)\xi_c \tag{19}$$

where

$$a = \frac{v_{O2,g}}{v_{O2,g} + v_{O2,c}} \tag{20}$$

Another measure of the total reaction extent can be obtained by considering the total heat evolved from the afterburn reactions. The heat evolved from the gas phase, Q_g, and condensed phase, Q_c, reactions, respectively, will again be based on their individual reaction extents, as well as their heats of combustion ($\Delta H_{r,g}$ and $\Delta H_{r,c}$), where:

$$Q_g = n_{x,i}\Delta H_{r,g}\xi_g \tag{21a}$$

$$Q_c = n_{x,i}\Delta H_{r,c}\xi_c \tag{21b}$$

The total heat evolved in the fireball is simply the sum of these two equations. Again, if this is normalized by the maximum amount of heat that can be liberated, Q^*, a different, energy-weighted measure of the combined gas phase/condensed phase reaction extents, η, can be obtained.

$$\eta = \frac{Q}{Q^*} = b\xi_g + (1-b)\xi_c \tag{22}$$

where

$$b = \frac{\Delta H_{r,g}}{\Delta H_{r,g} + \Delta H_{r,c}} \tag{23}$$

Both of these equations describe the total, combined reaction extent, although for any given combination of ξ_g and ξ_c, they would not necessarily yield the same answer. The reason for this is that, although they are both linear combinations of ξ_g and ξ_c (the underlying reaction extents), they carry different weighting factors. Per mole of oxygen consumed, the gas phase reactions have a higher heat of reaction than do the condensed phase reactions. For

example, if the gas phase reactions were to occur preferentially, then more heat would be evolved than if the condensed phase reactions were preferred instead.

If the heats of reaction were exactly the same, there would be no way to tell if one reaction proceeded faster than the other. But this peculiar behaviour, where more or less heat is liberated, even though the same amount of oxygen has been consumed, actually leads to a way to discriminate between the two reactions and determine which one is going forward preferentially.

Since χ and η are simply linear combinations of the underlying reaction extents for the gas phase (ξ_g) and condensed phase (ξ_c) species, they can be expressed as a matrix operation:

$$\begin{bmatrix}\chi\\ \eta\end{bmatrix} = \begin{bmatrix}a & (1-a)\\ b & (1-b)\end{bmatrix}\begin{bmatrix}\xi_g\\ \xi_c\end{bmatrix} = \mathbf{A}\xi \tag{24}$$

The reaction extents can then be computed from χ and η simply by taking the matrix inverse, noting that its determinant is $|\boldsymbol{A}| = a - b$.

Thus the underlying reaction extents can be found directly, as long as χ and η are both known. For this inversion to be possible, however, the heats of reaction per mole of oxygen consumed must be different. If they are the same, the determinant in Eq. (24) would be zero, and the matrix in Eq. (24) would be singular. Even if the two are close, the large magnitudes of elements in the inverse matrix would mean that any errors with χ and η would be greatly magnified. As long as the differences in heat of reaction are large enough, though, this gives a powerful tool that allows the underlying reaction extents to be determined.

In addition to the underlying extents, the fractional reaction rate, f, can also be determined. The differential rate at which heat is evolved in the fireball can be obtained using Eq. (22) to yield:

$$d\eta = b\,d\xi_g + (1-b)\,d\xi_c \tag{25}$$

Relating this expression to the rate of oxygen consumption, using Eq. (17), yields:

$$d\eta = \frac{1}{n_{x,i}}\left[\frac{bf}{v_{o2,g}} + \frac{(1-b)(1-f)}{v_{O2,c}}\right] dn_{O2} \tag{26}$$

As χ is the ratio of the amount of oxygen that has been consumed in the fireball, to the total amount that stoichiometrically could be consumed (Eq. (19)), then the rate at which χ changes can also be related to the rate of oxygen consumption by:

$$d\chi = \frac{1}{n_{x,i}}\frac{1}{v_{O2,g} + v_{O2,c}}\, dn_{O2} \tag{27}$$

These last two expressions can be combined to obtain the following equation, which expresses the derivative of η with respect to χ in terms of f:

$$\frac{d\eta}{d\chi} = \frac{b}{a}f + \frac{1-b}{1-a}(1-f) \tag{28}$$

From a plot of η versus χ, therefore, the slope at any point is related to the fractional rate, f, at which oxygen is consumed in the gas phase reaction. Since the gas phase reactions release more energy per mole of oxygen consumed than the condensed phase reactions, a higher value for the slope means that the gas phase reactions are going forward preferentially, while a lower value means that the condensed phase reactions are preferred.

7. Detonation product combustion

7.1. Computing χ and η from data

Data from the calorimetry experiments can be transformed so that they can be expressed in terms of the energy-weighted and oxygen-weighted total reaction extents. In addition to the explosives, the tape that was used to hold the charge together had to be taken into account, as it also participated in the secondary combustion reactions, and as such also consumed oxygen and released heat. Its chemical composition was assumed to be one monomer of polyisobutylene adhesive, and two monomers of polyethylene backing, with cotton mesh and additives ignored [22]. Its heat of combustion was measured at 38.9 ± 0.4 kJ g^{-1} using a Parr Instruments model 1241 adiabatic bomb calorimeter.

The oxygen-weighted total reaction extent can be computed from measured values by:

$$\chi = \frac{n_{O2,i}}{(v_{O2,g} + v_{O2,c})n_{x,i} + v_{O2,dt}n_{dt,i}} \tag{29}$$

where $n_{dt,i}$ and $v_{O2,dt}$ are the number of moles and stoichiometric coefficient for oxygen for the tape, respectively.

For the energy-weighted total reaction extent, only the energy released during the secondary combustion reactions, and not the initial detonation, are of interest. Correcting for this, while taking into account the energy released from the tape as well, yields:

$$\eta = \frac{Q_{meas} - n_{x,i}\Delta H_{d,x}}{n_{x,i}\Delta H_{ab,x} + n_{dt,i}\Delta H_{c,dt}} \tag{30}$$

7.2. Applying thermochemical model to data

The values for the energy-weighted and oxygen-weighted total reaction extent are plotted against one another in Fig. 4. The black earth trials were not included in this plot, since Eqs. (29) and (30) could not directly account for its combustion. Independent of the type of explosive, the data points are fairly tightly grouped together, but the values for the energy-weighted total reaction extent for each trial was consistently less than the corresponding oxygen-weighted total reaction extent, especially for points in the middle regions of the plot. What this is starting to show is that the condensed phase and gaseous phase detonation products are being consumed at different rates. After all, these two types of detonation product have different heats of reaction, and in oxygen limited environment, if the material with the lower heat of reaction is consumed preferentially, then less heat would be liberated for each unit of oxygen consumed.

The next step is to try to represent the underlying physical process with a statistical model relating heat liberation to oxygen consumption. To reflect physical circumstances, the proposed function must pass through both the points (0,0) and (1,1), meaning that no heat can be liberated before any oxygen is consumed, and that if all the fuel is consumed (meaning a stoichiometric amount of oxygen has been consumed), then a maximum amount of heat has been released. The function must also be continuous, and there should be no discontinuities in heat release, though discontinuities in the derivative of heat release are acceptable.

In the plot shown in Fig. 4, the data in the region of about $\chi > 0.4$ follow a linear relationship. In spite of a gap in the data, the having a continuous overarching function is a physical constraint. One can assume, though, that if the function is linear when $\chi > 0.4$, then it may also be linear when $\chi < 0.4$ as well. One way to model these data, therefore, would be with a piecewise linear equation that would leave the origin with a relatively shallow slope, and then at a certain critical point turn upward with a

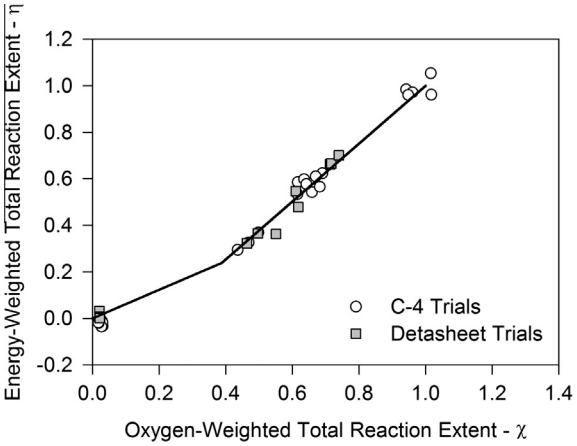

Fig. 4. Piecewise linear fit to the weighted total reaction extent data.

steeper slope in order to go to the point (1,1). This latter portion would pass through all of the measured data points, and would have a slope, $d\eta/d\chi > 1$.

The derivative of a piecewise linear function is constant over specific domains, but changes between different constant values when crossing from one domain to another. Therefore, $d\eta/d\chi$ is initially constant, but then changes to a higher value once a critical reaction extent, χ_{crit}, is crossed. Recalling from Eq. (28) that $d\eta/d\chi$ is a function of the fractional rate, f, at which oxygen is consumed by the gas phase reactions, the implication of the model is that f must also change from one value to another after the critical reaction extent is achieved.

$$f = \begin{cases} f_1 & \chi \leqslant \chi_{crit} \\ f_2 & \chi > \chi_{crit} \end{cases} \tag{31}$$

The two main competing reactions that occur in the secondary fireball are the condensed phase reactions, which involve heterogeneous gas-particle combustion, and gas phase reactions, which involve homogeneous reaction between the gaseous detonation products and atmospheric oxygen. If the condensed phase reactions are initially faster than the gas phase reactions, it is possible that they are so much faster that the gas phase reactions are negligible in comparison. This leads to the hypothesis that f is a step function where $f_1 \approx 0$ and $f_2 \approx 1$, so that when the condensed phase reactions happen, they are so much faster ($r_c \gg r_g$) that they consume all the oxygen and go to completion before the gas phase reactions have a chance to proceed to any significant extent. It is only when $r_c \to 0$, because most of the condensed phase species have been consumed, that heat release due to the gas phase reactions can be observed.

The linear regression of the data in Fig. 4, excluding the points near the origin, was carried out, and plotted. This regression was constrained to pass through the point (1,1), and produces a fit with an R^2 value of greater than 99% that is an excellent fit for the combined C-4/Detasheet data. Recalling Eq. (28), and taking $f = 1$, the slope obtained from the linear regression is equal to:

$$\left(\frac{d\eta}{d\chi}\right)_g = \frac{b}{a} = 1.24 \pm 0.02 \tag{32}$$

Conversely, taking $f = 0$, the slope of the portion of the piecewise linear equation that leaves the origin, and corresponding to combustion of the condensed phase, is:

$$\left(\frac{d\eta}{d\chi}\right)_c = \frac{1-b}{1-a} = 0.62 \pm 0.05 \tag{33}$$

where the value of 0.62 ± 0.05 could be calculated from the slope in Eq. (32) knowing the ratio, $\Delta H_{r,g}/\Delta H_{r,c}$ by the formula:

$$\left(\frac{d\eta}{d\chi}\right)_c = \left[1 + \frac{\Delta H_{r,g}}{\Delta H_{r,c}} \cdot \left(1 - \left(\frac{d\eta}{d\chi}\right)_g^{-1}\right)\right]^{-1} \tag{34}$$

This calculation only uses information from the data in the $\chi > 0.4$ region of Fig. 4, from which the slope in Eq. (32) was calculated, as data are very sparse in the region where $\chi < 0.4$.

With this, the slopes of both sections of the piecewise linear equation are known. In addition, since the lower section must pass through the origin, (0,0), since the upper section must pass through the point (1,1), and since the function must be continuous, the two linear sections must intersect at the critical values for the oxygen and energy-weighted total reaction extents:

$$\chi_{crit} = \frac{\left(\frac{d\eta}{d\chi}\right)_g - 1}{\left(\frac{d\eta}{d\chi}\right)_g - \left(\frac{d\eta}{d\chi}\right)_c} = 0.39 \pm 0.05 \tag{35a}$$

$$\eta_{crit} = \frac{1 - \left(\frac{d\eta}{d\chi}\right)_g^{-1}}{\left(\frac{d\eta}{d\chi}\right)_c^{-1} - \left(\frac{d\eta}{d\chi}\right)_g^{-1}} = 0.24 \pm 0.07 \tag{35b}$$

The piecewise linear equation for this system, which relates the energy-weighted to the oxygen-weighted total reaction extents, is therefore:

$$\eta = \begin{cases} (0.62 \pm 0.05)\chi & \chi \leqslant 0.39 \pm 0.05 \\ (1.24 \pm 0.02)(\chi - 1) + 1 & \chi > 0.39 \pm 0.05 \end{cases} \tag{36}$$

The critical transition point occurs for χ when it is equal to the fraction of the total oxygen that can be consumed by the condensed phase reactions over the amount of oxygen that can be consumed in total by both reactions. This point occurs for η when it is equal to the fraction of total heat that can be liberated by the condensed phase reactions over the total heat of afterburn.

Likewise, using the relationship between the different slope values and the ratios of a and b in Eqs. (32) and (33), the critical transition values can be simplified to:

$$\chi_{crit} = \frac{\frac{a}{b} - 1}{\frac{a}{b} - \frac{1-a}{1-b}} = 1 - a \tag{37a}$$

$$\eta_{crit} = \frac{1 - \frac{b}{a}}{\frac{1-b}{1-a} - \frac{b}{a}} = 1 - b \tag{37b}$$

As a is the stoichiometric coefficient for oxygen for the gas phase reactions, normalized by the total oxygen stoichiometric coefficient for the gas and condensed phase species together, and b is the same ratio, but for the heat of combustion of the gas phase species, Eq. (37) has shown that these can each be calculated directly from the estimated values of $(d\eta/d\chi)_g$ and $(d\eta/d\chi)_c$ to yield:

$$a = \frac{\nu_{O2,g}}{\nu_{O2,g} + \nu_{O2,c}} = 0.61 \pm 0.05 \tag{38}$$

and,

$$b = \frac{\Delta H_{r,g}}{\Delta H_{r,g} + \Delta H_{r,c}} = 0.76 \pm 0.07 \tag{39}$$

Since the total heat of reaction of all products, and total oxygen consumption of all products is known in advance, the heat of

reaction per mole of oxygen for the gas phase and condensed phase reactions can be obtained from the estimated values of $(d\eta/d\chi)_g$ and $(d\eta/d\chi)_c$ as well:

$$\frac{\Delta H_{r,g}}{\nu_{O2,g}} = \frac{\Delta H_{r,g} + \Delta H_{r,c}}{\nu_{O2,g} + \nu_{O2,c}} \cdot \left(\frac{d\eta}{d\chi}\right)_g = 520 \pm 10 \text{ kJ mol}^{-1} \quad (40)$$

and,

$$\frac{\Delta H_{r,c}}{\nu_{O2,c}} = \frac{\Delta H_{r,g} + \Delta H_{r,c}}{\nu_{O2,g} + \nu_{O2,c}} \cdot \left(\frac{d\eta}{d\chi}\right)_c = 260 \pm 20 \text{ kJ mol}^{-1} \quad (41)$$

Comparing these values to the heats of reaction per mole of oxygen consumed for individual gas phase and condensed phase species (given in Table 6) demonstrates that they likely represent the average values for the multi component reactions.

The fact that correct average heats of reaction were obtained is the first sign that the f-step function hypothesis is correct. It can be further confirmed by trying to obtain estimates for the reaction extent. With estimates for a and b available, it is possible to calculate estimates for the reaction extents of individual species, ξ_g and ξ_c, through the inversion of Eq. (24). These results are shown in Fig. 5 below for both C-4 and detasheet, and although there is some scatter (as division by $a - b$ in the determinant yields large parameters in the inverse matrix), the points still have behaviour consistent with the hypothesized underlying mechanism.

The largest amount of scatter is seen in the points corresponding to the condensed phase reaction extent. For these, the points with $\chi > 0.4$ appear to be scattered ±30%, but are well distributed around $\xi_c = 1$. The points corresponding to the gas phase reaction extent are less scattered, and rise from $\xi_g \sim 0$, fairly linearly, toward the point (1,1), close to the extent that is predicted by the f-step function model. Despite the scatter in the data, though, the inversion further confirms the hypothesized underlying mechanisms, where the condensed phase reactions occur sufficiently quickly that they can go to completion before the gas phase reactions can proceed to any significant extent.

7.3. Addition of external combustible material

The results from the black earth trials have not been included in the analysis so far because, unlike the trials carried out with other soil types, black earth also participates in the fireball combustion. By mass, the trials were carried out with about four times as much soil as explosives (about 60 g versus 15 g). The quantity of combustible black earth, therefore, was far greater than the amount of detonation products. There was an overwhelmingly large quantity of combustible particulates in these trials. Since the particulates, as it has been found, react much faster, and given the limited amount of oxygen, one would expect that the contribution to heat release from the gas phase combustion would be negligibly small.

Table 6
Heats of reaction per mole of oxygen consumed for various components.

Component	Reaction	Heat of reaction (kJ mol^{-1})
Gas phase		
Carbon monoxide	$2CO + O_2 \rightarrow 2CO_2$	−566
Methane	$\frac{1}{2}CH_4 + O_2 \rightarrow \frac{1}{2}CO_2 + H_2O$	−445
Hydrogen	$2H_2 + O_2 \rightarrow 2H_2O$	−572
Ammonia	$\frac{4}{3}NH_3 + O_2 \rightarrow \frac{2}{3}N_2 + 2H_2O$	−510
Condensed phase		
Carbon	$2C_{(s)} + O_2 \rightarrow 2CO$	−221
Tape[a,b]	$\frac{1}{4}C_4H_8 + O_2 \rightarrow CO + H_2O$	−310
Black earth[a,b]	$C_2H_2O_1 + O_2 \rightarrow 2CO + H_2O$	−230

[a] Assumed composition. Tape: one monomer of polyisobutylene adhesive and two monomers of polyethylene backing; cotton mesh and additives ignored [22]. Black earth: simplified composition for mixture of humic and fulvic acids [23].

[b] Heat of reaction calculated from measured full heat of combustion to partial heat of reaction with carbon monoxide as product [20].

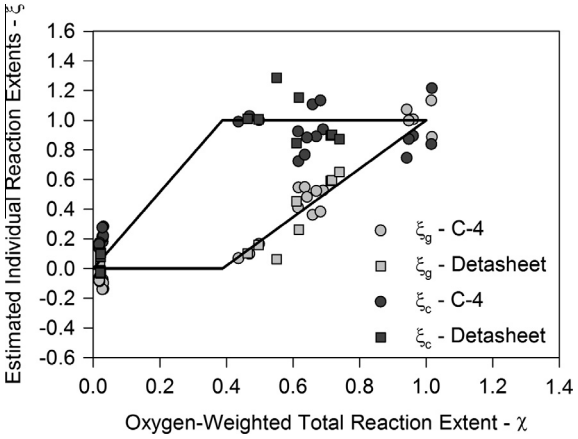

Fig. 5. Extent for gas phase and condensed phase reactions.

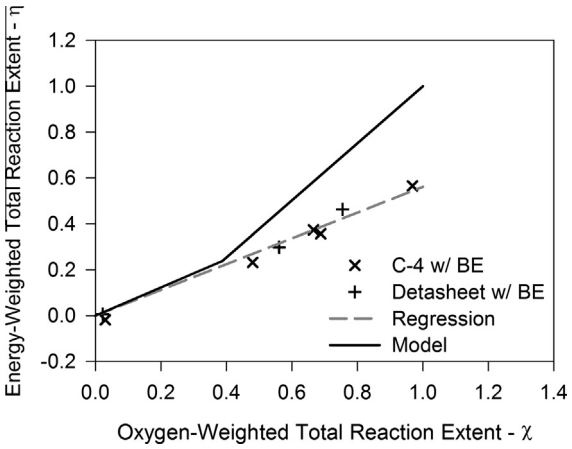

Fig. 6. Linear fit to black earth data.

Applying the same transformations in Eqs. (29) and (30) to the black earth trials, the data fall below the data points from trials carried out with other types of soil. However, as can be seen in Fig. 6, the black earth data points all lie of a straight line extending from the origin.

The slope of the line that passes through the black earth data points is 0.56 ± 0.02, which is very close to the slope of the lower portion of the piecewise linear fit, at 0.62 ± 0.05, that was obtained previously.

The heat of (partial) combustion of black earth per mole of oxygen consumed (about −230 kJ mol^{-1}) is in the same neighbourhood as that for other condensed phase products (about −260 kJ mol^{-1}). When the system was overwhelmingly full of combustible (soil) particles, the fact that essentially the same amount of heat release per mole of oxygen consumed was seen, as in the initial phase of the afterburn reactions, further confirms that gas-particle combustion occurs much more quickly than the gas–gas combustion.

8. Conclusion

By looking specifically at the secondary combustion reactions in the fireball, this paper has shown that, as the detonation products

mix together with the surrounding air, condensed phase detonation products react much faster than the gaseous phase species. Experiments employing a calorimeter have enabled thermochemical arguments to show this from the relationship between oxygen consumption and heat production.

The results from this paper imply that the condensed phase reactions are highly favoured. In the highly turbulent environment of an explosive fireball, where transport limitations control the progression of reactions, the fact that particles can deviate from the streamlines of circulating flows, and cross over into adjacent streams that contain the surrounding air, allows them to come into contact more efficiently with oxygen, and thus enhances the rate at which they are consumed. This effect is driven by the rotation of microscale turbulent eddies, and even for particles in the micron size range and lower, the level of turbulence that would be expected in an explosive fireball is more than enough to allow it to dominate gas mixing, which is diffusion-driven over the microscale interfaces between eddies.

This applies well for CHNO explosives, where carbonaceous soot can be readily consumed and the secondary combustion reactions are transport limited. Results may vary if kinetic and physical factors come more strongly into play, as may be the case for metalized explosives, or if the degree of turbulence is not as high. In the situation covered in this paper, though, the species that can mix with air the most effectively will react first, and here it is clear that particulates have an advantage over species in the gas phase.

Acknowledgments

This work was funded by the *Chemical, Biological, Radiological-Nuclear and Explosives (CBRNE) Research and Technology Initiative*, a program led by the Defence R&D Canada – Centre for Security Science, as well as the Canadian Forces Director General Nuclear Safety. The authors would also like to thank the ammunition technicians at Canadian Forces Base Kingston, Sgt. E. Lebreton and D. Breen, for their invaluable support during the experimental program.

References

[1] P.W. Cooper, Explosives Engineering, Wiley-VCH, New York, USA, 1996. pp. 24–27 and 117–133.
[2] A.E. Wildegger-Gaissmaier, ADF Health 4 (2003) 3–6.
[3] K. Balakrishnan, D. Genin, V. Nance, S. Menon, Shock Waves 20 (2) (2010) 147–162.
[4] K. Balakrishnan, S. Menon, Flow Turbulence Combust. 87 (2011) 639–671.
[5] H.L. Brode, Phys. Fluids 2 (2) (1959) 217–229.
[6] S.I. Ansimov, Y.B. Zeldovich, Pis. Z. Tekh. Fiz. 3 (1977) 1081–1084.
[7] A.L. Kuhl, R.E. Ferguson, A.K. Oppenheim, Arch. Combust. 19 (1–4) (1999) 67–89.
[8] D.L. Frost, Z. Zarei, F. Zhang, Instability of Combustion Products Interface from Detonation of Heterogeneous Explosives, International Colloquium on the Dynamics of Explosions and Reactive Systems, Montreal, Canada, 2005.
[9] K.L. McNesby, B.E. Homan, J.J. Ritter, Z. Quine, R.Z. Ehlers, B.A. McAndrew, Propellants, Explos., Pyrotech. 35 (2010) 57–65.
[10] R. Krasny, J. Comput. Phys. 65 (1986) 292–313.
[11] W.C. Hinds, in: Aerosol Technology: Properties, Behavior, and Measurement of Airborne Particles, second ed., Wiley-Interscience, New York, USA, 1999. pp. 42–62 and 75–97.
[12] S.K. Friedlander, in: Smoke Dust and Haze: Fundamentals of Aerosol Dynamics, second ed., Oxford University Press, New York USA, 2000, pp. 361–368.
[13] A. La Porta, G.A. Voth, A.M. Crawford, J. Alexander, E. Bodenschatz, Nature 409 (2001) 1017–1019.
[14] F.P. Incropera, D.P. DeWitt, T. L Bergman, A.S. Lavine, Fundamendals of Heat and Mass Transfer, sixth ed., Wiley, Hoboken, USA, 2007. pp. 879–885.
[15] N. de Nevers, Fluid Mechanics for Chemical Engineers, third ed., McGraw-Hill, New York, USA, pp. 546–554.
[16] L.S. Lebel, P. Brousseau, L.S. Erhardt, W.S. Andrews, J. Appl. Mech. 80 (3) (2013). 031702-1 – 031702-6.
[17] P.E. Liley, G.H. Thomson, D.G. Friend, T.E. Daubert, E. Buck, Physical and Chemical Data, in: R.H. Perry, D.W. Green (Eds.), Perry's Chemical Engineers' Handbook, seventh ed., McGraw Hill, New York, USA, 1997. pp. 2.195–2.198 and 2.306–2.307.
[18] P.D. Katsabanis, Development of a Detonation Calorimeter to Measure the Heat of Detonation of High Explosives, Queen's University, 1993.
[19] L.S. Lebel, P. Brousseau, L.S. Erhardt, W.S. Andrews, Intl. J. Energy Mater. Chem. Propul. 10 (4) (2011) 351–364.
[20] L.S. Lebel, Aerosolization and Soil Entrainment in Explosive Fireballs, PhD thesis, Royal Military College of Canada, 2012.
[21] L. Fried, P. Souers, CHEETAH: A Next Generation Thermochemical Code, Report No. UCRL-ID-117240, Lawrence Livermore National Laboratory, 1994.
[22] D. Satas, Handbook of Pressure Sensitive Adhesives Technology, second ed., Van Nostrand Reinhold, New York, USA, 1989.
[23] Encyclopaedia Britannica Online, Humus, <http://www.britannica.com/EBchecked/topic/276408/humus>, 2012 (accessed 09.02.12).